Radiation pressure acceleration of ultrathin foils

2010 New J. Phys. 12 045013

(http://iopscience.iop.org/1367-2630/12/4/045013)

New Journal of Physics
The open-access journal for physics

Radiation pressure acceleration of ultrathin foils

Andrea Macchi[1,2,6], **Silvia Veghini**[1], **Tatyana V Liseykina**[3,4] **and Francesco Pegoraro**[1,5]

[1] Department of Physics 'E. Fermi', Largo B Pontecorvo 3, 56127 Pisa, Italy
[2] CNR, Istituto Nazionale di Ottica (INO), Pisa, Italy
[3] Max Planck Institute for Nuclear Physics, Heidelberg, Germany
[4] Institute of Computational Technologies, SD-RAS, Novosibirsk, Russia
[5] Consorzio Nazionale Interuniversitario per le Scienze Fisiche della Materia (CNISM), unità di ricerca di Pisa, Italy
E-mail: macchi@df.unipi.it

New Journal of Physics **12** (2010) 045013 (18pp)
Received 13 October 2009
Published 30 April 2010
Online at http://www.njp.org/
doi:10.1088/1367-2630/12/4/045013

Abstract. The acceleration of sub-wavelength, solid-density plasma foils by the ultraintense radiation pressure of circularly polarized laser pulses is investigated analytically and with simulations. An improved 'Light Sail' or accelerating mirror model, accounting for nonlinear self-induced transparency effects, is used for estimating the optimal thickness for acceleration. The model predictions are in good agreement with one-dimensional simulations. These latter are analyzed in detail to unfold the dynamics and self-organization of electrons and ions during the acceleration. Two-dimensional simulations are also performed to address the effects of target bending and of laser intensity inhomogeneity.

[6] Author to whom any correspondence should be addressed.

Contents

1. Introduction

Present-day laser systems may deliver at their focal spot intensities up to $10^{22}\,\mathrm{W\,cm^{-2}}$, and possibly even higher in the near future. The radiation pressure on a reflecting object corresponding to such intensities would exceed terabar values, driving strong compression and acceleration of matter. A few experiments have already given some evidence of strong radiation pressure (or ponderomotive) effects in various regimes [1]–[3]. The possibility to develop laser-driven sources of high-energy ions based on radiation pressure acceleration (RPA) is of particular interest. Theoretical studies [4]–[6] have shown that in the interaction with ultrathin (sub-micrometric) foils at intensities exceeding $10^{23}\,\mathrm{W\,cm^{-2}}$, the dominant mechanism of ion acceleration may be RPA instead of target normal sheath acceleration (TNSA), which has been intensively investigated experimentally (see [7] for a review). A regime of radiation pressure dominance may also exist at lower intensities, if circular polarized (CP) laser pulses at perpendicular incidence on the target are used. In such conditions, TNSA may be ruled out by the strong quenching of high-energy electron generation for CP pulses [8]. The regime of RPA with CP pulses has been recently investigated in many theoretical papers for different laser and target conditions, including thick targets ('hole boring' regime) [8]–[13], structured or composite targets [14]–[18], and ultrathin foils [19]–[29]. The effects of elliptical polarization were also studied [30, 31]. First experimental results were communicated recently [32]–[34].

In this paper, we focus on ultrathin foil targets. Although experimentally challenging, such a regime appears to be feasible due to the present possibility of both manufacturing targets as thin as a few nanometers, e.g. diamond-like carbon (DLC) foils, and avoiding early disruption of such targets by prepulse effects thanks to the use of techniques such as the plasma mirror to obtain extremely 'clean' pulses [35]. Early theoretical studies both for linearly polarized pulses in the radiation pressure-dominated regime [4] and for CP pulses at lower intensities [19]–[22] suggested that an ultrathin foil may be accelerated as a whole, leading to a monoenergetic spectrum of ions. In addition, the acceleration process is highly efficient and the energy per nucleon scales favorably with the laser pulse energy. These features are in agreement with the predictions of the simplest model of thin-foil acceleration, which assumes the thin foil target to be a perfectly reflecting, undeformable, plane mirror boosted by the radiation pressure of an electromagnetic (EM) plane wave (corresponding to the laser pulse) at perpendicular incidence.

This regime of RPA has also been named 'Light Sail' (LS), and in the following we refer to the 'accelerating mirror' model as the LS model.

This paper is organized as follows. In section 2, we present an analytical model that improves the basic LS model by including the effect of the nonlinear self-induced transparency (SIT) of the foil at 'relativistically' strong laser intensities. It is found that SIT effects determine an 'optimal' value of the foil thickness for which, given a laser pulse, the foil velocity is highest. The predictions of the model are found to be in good agreement with one-dimensional (1D) particle-in-cell (PIC) simulations for what concerns the energy of the spectral peak of 'monoenergetic' ions and the conversion efficiency.

In section 3, the dynamics of thin-foil RPA is analyzed in 1D PIC simulations. It is found that the distribution of electrons and ions undergoes a dynamic self-organization to maintain an equilibrium condition for electrons where the electrostatic and ponderomotive forces balance each other. It is found that in general the spectral peak contains just a fraction of the total ions, the actual value depending on the target and pulse parameters.

In the final section 4, the acceleration of foils with thicknesses close to the 'optimal value' is further investigated with two-dimensional (2D) simulations, addressing the effects of target bending and of laser intensity inhomogeneity.

2. Thin-foil modeling

2.1. Review of the LS model

The LS model takes into account an EM plane wave of frequency ω and intensity $I = I(t)$, perpendicularly incident on a foil of mass density ρ, thickness ℓ and reflectivity $R = R(\omega)$. In the rest frame of the foil, neglecting dissipative effects, the radiation pressure is given by

$$P_{\mathrm{rad}} = 2R\frac{I}{c}. \tag{1}$$

Note that equation (1) is different from the known expression for the case of incidence on a semi-infinite medium

$$P_{\mathrm{rad}} = (1+R)\frac{I}{c}, \tag{2}$$

which does not vanish if $R = 0$ because the transmitted wave does not leave the target and deliver all its momentum there.

By a Lorentz transformation of the force on the foil and of the intensity and frequency of the EM wave, the following equations of motion for the foil in the laboratory frame are obtained:

$$\frac{\mathrm{d}}{\mathrm{d}t}(\beta\gamma) = \gamma^3\frac{\mathrm{d}\beta}{\mathrm{d}t} = \frac{2I(t-X/c)}{\rho\ell c^2}R(\omega')\frac{1-\beta}{1+\beta}, \tag{3}$$

$$\frac{\mathrm{d}X}{\mathrm{d}t} = \beta c, \tag{4}$$

where $\beta = V/c$ is the velocity of the foil in units of the speed of light c, $\omega' = \omega\sqrt{(1-\beta)/(1+\beta)}$ is the EM wave (laser) frequency in the rest frame and $\gamma = (1-\beta^2)^{-1/2}$.

For $R = 1$, i.e. taking the foil as a perfectly reflecting mirror, the model yields a simple solution for $\beta = \beta(w)$, where $w = t - X/c$ is the retarded time, as a function of the pulse fluence $\mathcal{F}$ (the pulse energy per unit surface) [36, 37]:

$$\beta(w) = \frac{[1+\mathcal{E}(w)]^2 - 1}{[1+\mathcal{E}(w)]^2 + 1}, \tag{5}$$

$$\mathcal{E}(w) = \frac{2\mathcal{F}(w)}{\rho \ell c^2}, \qquad \mathcal{F}(w) = \int_0^w I(w')\,\mathrm{d}w'. \tag{6}$$

This expression can also be retrieved from the more general derivation given in section 2.3. The corresponding energy per nucleon is

$$E(w) = m_\mathrm{p}c^2[\gamma(w) - 1] = m_\mathrm{p}c^2 \frac{\mathcal{E}^2(w)}{2[\mathcal{E}(w)+1]}. \tag{7}$$

The instantaneous efficiency η, i.e. the ratio between the mechanical energy delivered to the foil and the incident pulse energy, is also a simple function of β [36, 37] or, equivalently, of $\mathcal{E}$:

$$\eta = \frac{2\beta(w)}{1+\beta(w)} = 1 - \frac{1}{[\mathcal{E}(w)+1]^2}. \tag{8}$$

Thus, $\eta \to 1$ when $\beta(w) \to 1$, i.e. when $\mathcal{E} \to \infty$.

The final velocity of the foil β_f and the corresponding energy per nucleon E_n are obtained trivially by rewriting equations (5)–(7) as a function of the total energy, i.e. by taking $\mathcal{E} = \mathcal{E}(\infty)$. In practical units,

$$\mathcal{E} \simeq 2.2 \frac{\mathcal{F}}{10^8\,\mathrm{J\,cm^{-2}}} \left(\frac{\rho}{1\,\mathrm{g\,cm^{-3}}}\right)^{-1} \left(\frac{\ell}{10\,\mathrm{nm}}\right)^{-1}. \tag{9}$$

It is also useful to rewrite $\mathcal{E}$ as a function of the relevant dimensionless parameters: the amplitude of the pulse $a_0 = \sqrt{I/m_\mathrm{e}c^3 n_\mathrm{c}}$ (with $n_\mathrm{c} = m_\mathrm{e}\omega^2/4\pi e^2$ the cutoff density), the surface density $\zeta = \pi(n_\mathrm{e}/n_\mathrm{c})(\ell/\lambda)$ (with $\lambda = 2\pi c/\omega$ the laser wavelength) and the duration of the laser pulse τ in units of the laser period $T = 2\pi/\omega = \lambda/c$. By estimating the total fluence $\mathcal{F} \simeq I(T\tau) = m_\mathrm{e}c^3 n_\mathrm{c} T(a_0^2\tau)$, we obtain for $\mathcal{E}$

$$\mathcal{E} \simeq \frac{2m_\mathrm{e}c^2 n_\mathrm{c} a_0^2 \tau \lambda}{m_\mathrm{i} n_\mathrm{i} \ell c^3} = 2\pi \frac{Z}{A}\frac{m_\mathrm{e}}{m_\mathrm{p}}\frac{a_0^2\tau}{\zeta}. \tag{10}$$

Figure 1 shows β_f and E_n as a function of $a_0^2\tau$ and ζ ($Z/A = 1/2$ has been assumed). To convert from/to practical units, for a laser wavelength $\lambda = 0.8\,\mu$m and a fully ionized DLC target ($\rho = 2.2\,\mathrm{g\,cm^{-3}}$, $n_\mathrm{e}/n_\mathrm{c} = 384$), we find $a_0^2\tau = 1.73\mathcal{F}/(10^4\,\mathrm{J\,cm^{-2}})$ and $\zeta = 1.5\ell/(1\,\mathrm{nm})$.

2.2. Nonlinear reflectivity

To include the effects or partial reflectivity ($R < 1$) and SIT into the LS model, we first look for a suitable analytical expression of R. We use the model of a delta-like 'thin foil' [38], i.e. a plasma slab located at $x = 0$ with electron density $n_\mathrm{e}(x) = n_0\ell\delta(x)$. The model gives the following expression for R in the rest frame of the foil:

$$R = \frac{1}{1+\zeta^{-2}\Gamma^2}, \tag{11}$$

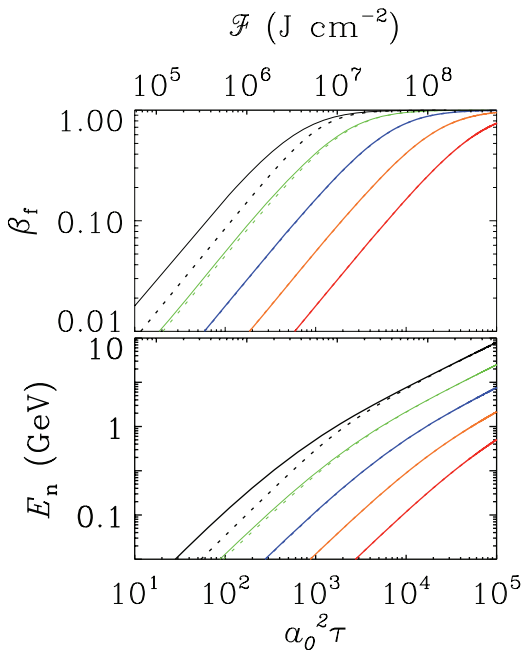

Figure 1. Analytical results from the LS model. The final velocity of the foil β_f and the corresponding energy per nucleon E_n are given as a function of the dimensionless pulse fluence $a_0^2\tau$ and for the values of surface density of the foil $\zeta = 1$ (black line), 3.16 (green), 10 (blue), 31.6 (orange) and 100 (red). The values on the upper horizontal axis give the fluence in J cm^{-2} corresponding to $a_0^2\tau$ for $\lambda = 0.8\,\mu$m. For a DLC target, $\zeta = 2.6\ell/(1\,\text{nm})$. The solid lines correspond to equation (5) i.e. to the case of a 'perfect' mirror with reflectivity $R = 1$. The dotted lines correspond to equation (17) where the effects of pulse transmission through the foil have been taken into account (for $\zeta \geqslant 10$, solid and dotted lines cannot be distinguished).

$$\Gamma = \frac{1 + a_0^2 - \zeta^2}{2} + \sqrt{\left(\frac{1 + a_0^2 - \zeta^2}{2}\right)^2 + \zeta^2}, \tag{12}$$

which is very well approximated by

$$R \simeq \begin{cases} 1/(1 + \zeta^{-2}) & (a_0 < \sqrt{1 + \zeta^2}), \\ \zeta^2/a_0^2 & (a_0 > \sqrt{1 + \zeta^2}). \end{cases} \tag{13}$$

Note that Γ is the relativistic factor for electrons in the thin foil (calculated self-consistently with the EM fields). It is thus apparent that the SIT is due to the relativistically increased inertia of electrons, as m_e is replaced by $m_e\Gamma$ in their equation of motion. The expression for $a_0 < \sqrt{1 + \zeta^2}$ corresponds to that obtained in the linear regime, i.e. for sub-relativistic intensities.

Equations (11) and (13) for R are both plotted in figure 2, showing that the transition from the linear to the nonlinear regime is quite sharp and that equation (13) provides an excellent approximation. We may thus define a threshold condition for relativistic SIT as $a_0 = \sqrt{1 + \zeta^2} \simeq \zeta$ when $\zeta \gg 1$, i.e. in most cases of interest. Combining equations (1) and (13), the total radiation pressure P_{rad} on the target becomes *independent* of a_0 for $a_0 > \zeta$. Thus, $a_0 \simeq \zeta$

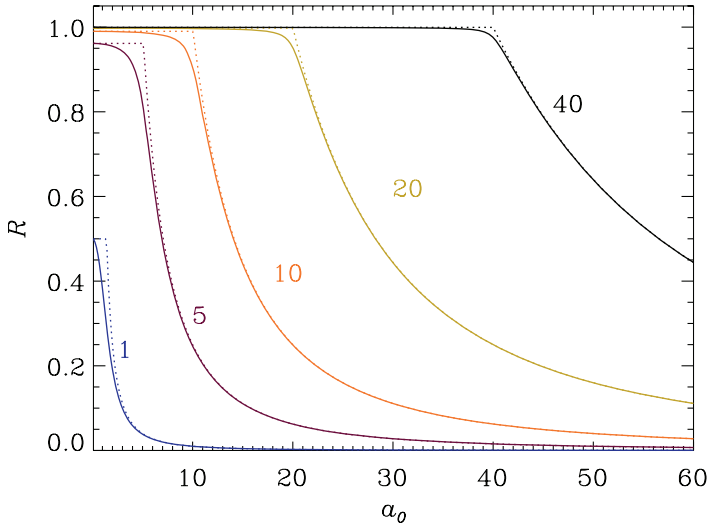

Figure 2. Nonlinear reflectivity R as a function of incident wave amplitude a_0 and for several values of the 'optical thickness' ζ. Thick and dashed lines correspond to the 'exact' formula (11) and to its approximation (13), respectively.

gives the condition of maximum radiation pressure on the (immobile) foil, and one would expect the RPA of the foil to saturate for $a_0 > \zeta$. Actually, simulations show that in this regime the interaction is rather dominated by the effect of expulsion of electrons from the foil, leading to a transition from RPA to a Coulomb explosion [28]. Hence, the LS model is appropriate for $a_0 < \zeta$.

2.3. *Improved LS formula*

According to equation (11), the reflectivity R is independent of a_0 in the $a_0 < \sqrt{1+\zeta^2}$ range, and for $\zeta \gg 1$, corresponding to most cases of experimental relevance, $R \simeq 1$ is a very good approximation. Nevertheless, thin-foil manufacturing technology seems able even to approach values of ζ not much larger than unity; hence it is of some interest to consider how the LS formulae are modified in the $a_0 > \zeta \gtrsim 1$ regime.

Using $R \simeq (1+\zeta^{-2})^{-1}$ and switching to the retarded time w, equation (3) becomes

$$\frac{\mathrm{d}\beta}{\mathrm{d}w} = \frac{2}{\rho\ell c^2} I(w)\gamma^{-3}(1+\beta)^{-1}\left(1+\zeta^{-2}\frac{1-\beta}{1+\beta}\right) \tag{14}$$

(note that $\mathrm{d}w = (1-\beta)\mathrm{d}t$). By switching to the variable $b(w) = \sqrt{(1-\beta)/(1+\beta)}$, we obtain

$$b^{-2}(w)\left[1+b^2(w)\zeta^{-2}\right]\frac{\mathrm{d}b}{\mathrm{d}w} = -\frac{2}{\rho\ell c^2} I(w), \tag{15}$$

which can be integrated with the initial condition $b(0) = 1$, corresponding to $\beta(0) = 0$, to yield

$$b^{-1}(w) - 1 - \zeta^{-2}b(w) + \zeta^{-2} = \frac{2}{\rho\ell c^2}\int_0^w I(w')\,\mathrm{d}w' = \mathcal{E}(w). \tag{16}$$

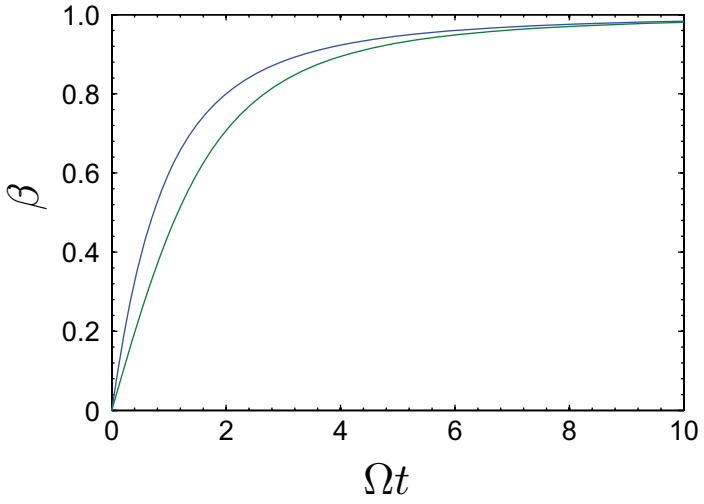

Figure 3. Foil velocity as a function of Ωt defined in (18) for $\zeta = 1$ (green lower curve) and for $\zeta^2 = \infty$, i.e. a perfectly reflecting foil (blue upper curve).

By solving (16) for $b(w)$ and rewriting the result for β, we obtain

$$\beta(w) = \frac{[1+\mathcal{E}(w)-\zeta^{-2}]^2\left(1+\sqrt{1+4\zeta^{-2}[1+\mathcal{E}(w)-\zeta^{-2}]^{-2}}\right)+2\zeta^{-2}-2}{[1+\mathcal{E}(w)-\zeta^{-2}]^2\left(1+\sqrt{1+4\zeta^{-2}[1+\mathcal{E}(w)-\zeta^{-2}]^{-2}}\right)+2\zeta^{-2}+2}. \tag{17}$$

In the limit of $\zeta \to \infty$, i.e. $R \to 1$, one recovers equation (5). As shown in figure 1, the difference between (5) and (17) (and between the corresponding energies) is important for $\zeta \sim 1$.

For a constant intensity I, i.e. for a 'flat-top' temporal profile of the laser pulse, the fluence can be written as a function of time as

$$\mathcal{E}(t) = \frac{2It}{\rho\ell c^2} = 2\pi\frac{Z}{A}\frac{m_e}{m_p}\frac{a_0^2}{\zeta}\frac{t}{T} \equiv \Omega t, \tag{18}$$

where T is the period of the laser radiation. In this case, explicit analytical expressions for $\beta(t)$ and $X(t)$ can be given as a function of ζ and Ωt [39]. The result for $\beta(t)$ is shown in figure 3 for the two cases $\zeta = 1$ and $\zeta = \infty$. The latter corresponds to the known solution for a perfectly reflecting mirror [4, 21], which is formally identical to the solution of the longitudinal motion of a charge during Thomson scattering from a plane wave [40].

2.4. Optimal thickness for ion acceleration

We now use the LS model with SIT effects included to provide an estimate for the value of foil surface density ζ_{max} (corresponding to thickness ℓ_{max} for a given target material), which, for a given laser pulse, leads to the highest foil velocity. In the regime of sub-relativistic intensity, ζ_{max} may be obtained by differentiating (17) with respect to ζ at fixed pulse fluence. However, for very high intensities, ζ_{max} is ultimately determined by SIT effects; thus the complete nonlinear expression for R (11) must be used. In the LS equation of motion (3), the expression for $R(\omega')$

now reads

$$R(\omega') = R(\beta) = \frac{1}{1+\zeta^{-2}\Gamma^2(\beta)(1-\beta)/(1+\beta)}, \tag{19}$$

$$\Gamma = \frac{1+a_0^2-\zeta^2(1+\beta)/(1-\beta)}{2} + \sqrt{\left(\frac{1+a_0^2-\zeta^2\frac{1+\beta}{1-\beta}}{2}\right)^2 + \zeta^2\frac{1+\beta}{1-\beta}}. \tag{20}$$

By using the variable $b(w)$ as in equation (15), we now obtain

$$[b^{-2}(w)+\Gamma^2(b)\zeta^{-2}]\frac{\mathrm{d}b}{\mathrm{d}w} = -\frac{2}{\rho\ell c^2}I(w), \tag{21}$$

which can be integrated for a constant intensity $I(w) = I$:

$$b^{-1}(w) - 1 - \zeta^{-2}\int_1^b \Gamma(b')\,\mathrm{d}b' = E(w). \tag{22}$$

Using the implicit equation (22), $b(w)$ and $\beta(w)$ can be obtained numerically. By differentiating (22) with respect to ζ at a fixed acceleration time τ (which should approximately correspond to the duration of the laser pulse), it can be shown [39] that $\zeta_{\max}$ lies in the interval

$$\sqrt{\left(\frac{\Omega\tau}{2\pi}\right)^2 + 1 + a_0^2} - \frac{\Omega\tau}{2\pi} < \zeta_{\max} < \sqrt{1+a_0^2}, \tag{23}$$

where Ω has been defined in (18). Equation (23) shows that for $\Omega\tau \ll 1$ the optimal thickness is $\zeta_{\max} \simeq \sqrt{1+a_0^2} \simeq a_0$, corresponding to the maximum radiation pressure on the immobile thin foil as found in section 2.2. As $\Omega\tau \gtrsim 1$ increases, e.g. for increasing pulse duration (keeping other parameters fixed), $\zeta_{\max}$ may become smaller than a_0. This effect may be ascribed to the increase of the reflectivity and the decrease of the intensity in the rest frame of the foil as it is accelerated to high values of β. Since $\Omega^{-1} \simeq 6\times 10^2\,\mathrm{T}(\zeta/a_0^2)$, this effect is relevant only for long (hundreds of periods) pulses. We may thus conclude that the condition of 'optimal' thickness, given by our improved LS model with SIT effects included for a pulse of constant amplitude a_0, is given by

$$\zeta_{\max} \simeq a_0. \tag{24}$$

In figure 4, the energy per nucleon E_n and the efficiency η obtained from the numerical solution of (22) for $\beta(\infty)$ are compared with the results of the 1D PIC simulations that were previously shown in figure 1 of [24]. In these simulations, η is calculated as the ratio between the total energy of the ions and the energy of the laser pulse. Both E_n and η are shown as a function of the target thickness ℓ and for three different values of the peak pulse amplitude a_0. For all simulations, $n_\mathrm{e} = 250 n_\mathrm{c}$, $Z/A = 1/2$ and the pulse has a full-width at half-maximum (FWHM) duration of 9 periods with a $\sin^2$ envelope for the field. A fairly good agreement between the model and simulations is found. Part of the discrepancy may be ascribed to the effect of the pulse envelope; for simulations with a flat-top envelope (i.e. a nearly constant amplitude), the observed 'optimal' thickness is in closer agreement with equation (24).

Several other authors give for the optimal thickness the same scaling of equation (24) but often with different numerical coefficients. Yan *et al* [23] give the following range,

$$\frac{\zeta}{\pi(1+R)^{1/2}} \sim a_0 \lesssim 2\zeta, \tag{25}$$

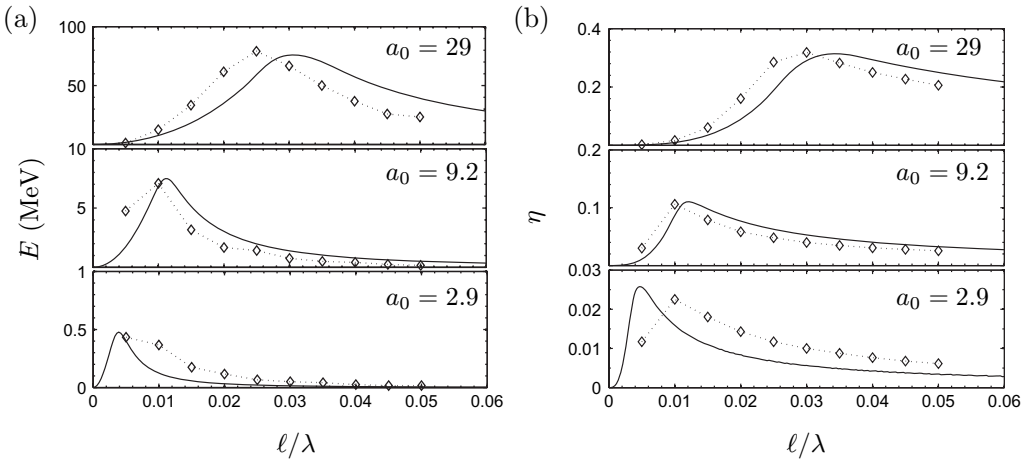

Figure 4. Energy per nucleon (a) and efficiency of energy conversion into ions (b) obtained as a function of target thickness ℓ and pulse amplitude a_0 for a laser pulse of duration $\tau = 9$ cycles and an electron density $n_e = 250 n_c$. The solid line gives the values corresponding to the numerical solution of (22) for β. The diamonds give the values obtained from parametric 1D PIC simulations.

using an argument of pressure balance but not accounting for SIT effects, since equation (2) is used for P_{rad}. A critical comment by Ji *et al* [41] about the $a_0 \lesssim 2\zeta$ condition appears to originate from a missing 2 factor [42]. Tripathi *et al* [26] give a condition identical to equation (24), accounting for the 'relativistic' modification of the plasma refractive index but using a calculation for a semi-infinite plasma profile. Finally, Esirkepov *et al* [5] observe in multi-parametric simulations a condition of the form $\zeta_{max} \simeq 3\pi + b\sqrt{I}$, where b is an appropriate constant factor, and notice its similarity with the SIT condition of a thin foil; however, the simulations are performed for linearly polarized pulses and for parameters not corresponding to the radiation pressure-dominated regime. An additional source of difference may be indeed the 2D (instead of 1D) nature of the simulations, as we also find ζ_{max} to be larger than indicated by equation (24) in 2D simulations (see section 4 below).

3. Electron and ion dynamics in one dimension

The comparison with 1D PIC simulation results shown in figure 4 shows that the simple LS model of section 2 is remarkably successful in predicting ion energy as a function of pulse energy and foil thickness. Moreover, for $a_0 \lesssim \zeta_{max}$ the further simplifying assumption of a totally reflecting foil ($R = 1$) is appropriate. The dynamics underlying the RPA of the thin foil is, however, more complex than what the simple 'mirror' model might suggest. Unfolding such dynamics with the help of simulations helps to explain why some of the observed features seem to be in contrast with the model assumptions. Such features have been discussed in [28]. In the following, we start by recalling the results we obtained in [28] and go a step further in the analysis.

The LS model assumes the foil as a 'rigid' object, so that all the ions and electrons move coherently at the same velocity $V = \beta c$ of the foil. However, the 1D simulations show that the spectral peak, centered at the energy predicted by the LS model, contains only a fraction of the

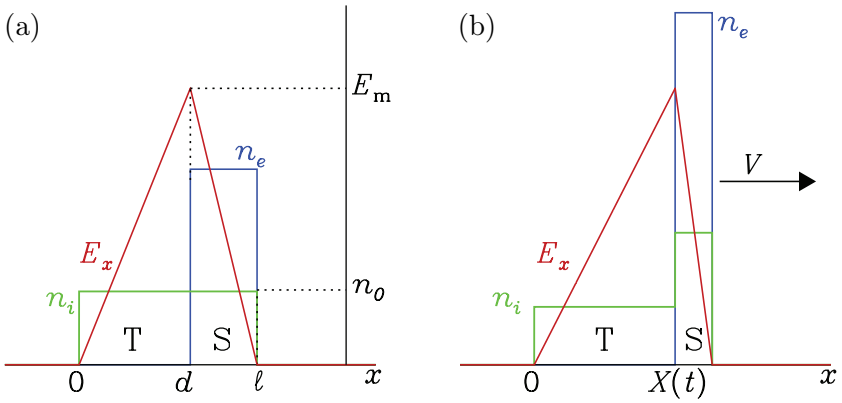

Figure 5. Cartoon showing how two ion populations are formed. The schematic profiles of the ion density n_i (green), electron density n_e (blue) and electrostatic field E_x (red) are shown at two different times. Part (a) corresponds to the early stage of the interaction where ions have not moved yet, so that their density equals the initial value n_0, and electrons have piled up under the action of the ponderomotive force f_p in the $d < x < \ell$ or 'Sail' (S) region. The $0 < x < d$ region of electron depletion is named as the 'Tail' (T) region. Part (b) shows the stage of ion acceleration. Ions in the T region are accelerated by their own space-charge field as in a Coulomb explosion, so that the ion density decreases in this region. Ions in the S region ($x > X(t)$) are bunched and accelerated by E_x, which in this region equals f_p/e, and move with the electrons at velocity V.

total number of the ions. Those 'monoenergetic' ions originate from a layer at the rear surface of the foil. The rest of the ions form an exponential-like 'pedestal' in the spectrum.

We explain the formation of the two ion populations with the help of the cartoon in figure 5. As the laser pulse impinges on the overdense plasma, the electrons are pushed by the steady ponderomotive force $\mathbf{f}_p$, whose integral over the whole target depth equals the radiation pressure. Thus, electrons pile up in the region $d < x < \ell$ of figure 5, which we call the 'Sail' region. The electron displacement generates the space-charge field $E_x \simeq f_p/e$ to balance the ponderomotive action. (If $R \simeq 1$, almost no electrons are pushed out of the foil, because the EM field and the ponderomotive force vanish at the rear surface of the foil; the electron compression does not change R in 1D since the product $n_e\ell$ is constant.) Ions in the Sail are accelerated and bunched by E_x [8, 28] and move together with electrons. The Sail is thus negatively charged during the acceleration because it contains all of the electrons in the foil but just a fraction $F \simeq 1 - d/\ell$ of the ions. An estimate for the condition of pressure equilibrium gives $F \simeq 1 - a_0/\zeta$, showing that F can be significantly smaller than unity as a_0 approaches ζ.

The analysis of 1D simulations confirms the above-described scenario. Typical snapshots of density and field profiles are shown in figure 6(a) for a simulation with $a_0 = 12$, $\tau = 9$, $n_e/n_c = 100$ and $\ell = 0.05$, so that $\zeta = 15.7$. Both a fine spatiotemporal resolution ($\Delta x = c\Delta t = \lambda/2000$) and a high number of particles per cell were used to resolve accurately the dynamics, and in particular the density variation that involves both the strong spiking in the Sail region and the rarefaction in the Tail region.

The Sail moves with a well-defined velocity V, so that ions in the Sail are monoenergetic. The velocity V satisfies the LS equation (3), where, according to the comparison with

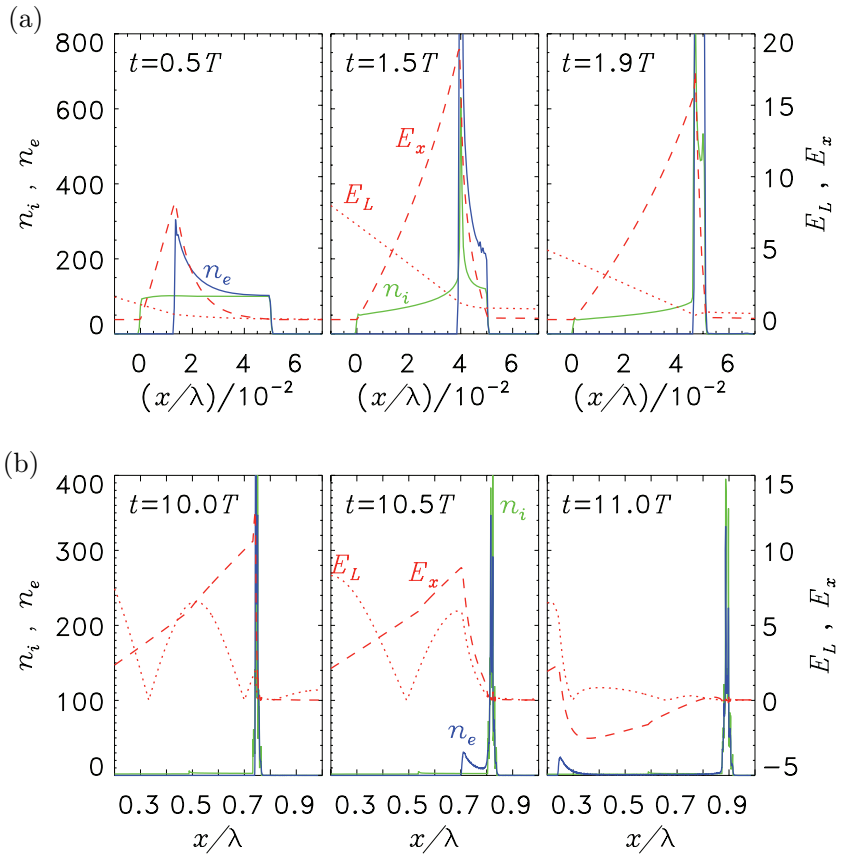

Figure 6. Snapshots from a 1D PIC simulation of the interaction of a laser pulse with a thin plasma slab. Ion density n_i (green), electron density n_e (blue), longitudinal electric field E_x (red, dashed) and pulse field amplitude $E_\mathrm{L} = \sqrt{E_y^2 + E_z^2}$ (red, dotted) are shown. Plots in row (a) correspond to the early stage of the interaction when electrons pile up at the rear side of the foil and a charged layer at the rear side is accelerated. Plots in row (b) correspond to later times when the laser pulse decouples from the foil and excess electrons are accelerated backward leaving the charged layer. Note that the scales of the x and $n_{\mathrm{e,i}}$ axes have been changed in (b) with respect to (a) for better visibility. The target left boundary is at $x = 0$ where the pulse impinges at $t = 0$. Times are normalized to the laser period T, fields to $E_0 = m_\mathrm{e}\omega c/e$ and densities to $n_\mathrm{c} = m_\mathrm{e}\omega^2/4\pi e^2$. The laser pulse has peak amplitude $a_0 = 12$ and a 'flat-top' profile with a duration of $9T$ (FWHM) and $1T$ rise and fall times, the foil thickness is $\ell = 0.05\lambda$, the electron density $n_\mathrm{e} = 100 n_\mathrm{c}$ and $Z/A = 1/2$.

simulations, the *total* thickness ℓ of the foil, i.e. the total mass, must be used. This may actually sound surprising because the Sail's mass is $\simeq F$ times the total mass and the total pressure on ions is lower than P_rad. In fact, in 1D the equilibrium condition for electrons is

$$\int (-e) n_\mathrm{e} E_x \, \mathrm{d}x = \int n_\mathrm{e} f_\mathrm{p} \, \mathrm{d}x = P_\mathrm{rad}, \tag{26}$$

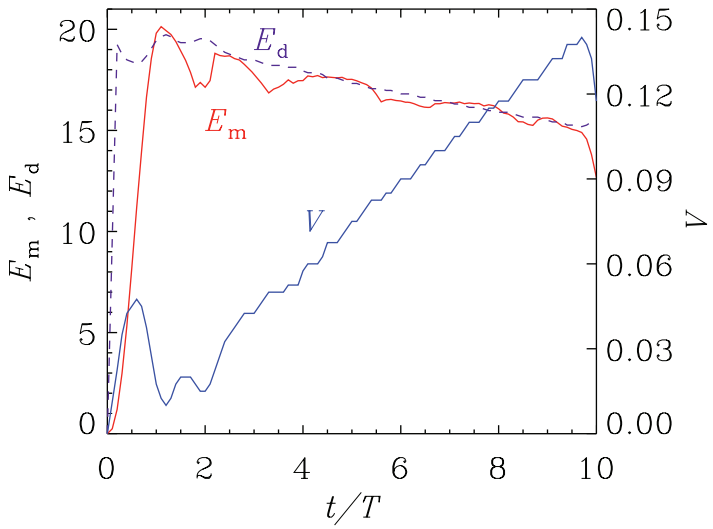

Figure 7. Red solid line: temporal evolution of the peak of the electrostatic field E_x from the same simulation of figure 6, $E_m(t) = E_x(x = X(t))$. Blue solid line: velocity of the peak position $V(t) = dX/dt$. Purple dashed line: function $E_d(t) = E_m(0)(1 - V/c)/(1 + V/c)$.

while the total electrostatic pressure P_{es} on ions is given by

$$P_{es} = \int Zen_i E_x \, dx \tag{27}$$

(the ponderomotive force on ions is smaller than f_p by a factor $\sim m_e/m_i$ and is thus negligible). Only in the case of local charge neutrality $Zn_i = n_e$, would we obtain $P_{es} = P_{rad}$. However, in the Sail, $Zn_i < n_e$, so that $P_{es} < P_{rad}$. The calculation of P_{es} from the approximate initial profiles of n_i and E_x (figure 5(a)) in equilibrium conditions shows that $P_{es} = FP_{rad}$ [28]; thus the equation of motion for the Sail can be written as

$$\frac{d}{dt}(\beta\gamma) = \frac{P_{es}}{\rho\ell Fc^2} = \frac{P_{rad}F}{\rho\ell Fc^2} = \frac{P_{rad}}{\rho\ell c^2}, \tag{28}$$

which is equivalent to equation (3).

In the $0 < x < d$ region, which we call the 'Tail' region, complete electron depletion occurs. In the Tail, ions are accelerated by their own space-charge field, as in a Coulomb explosion, resulting in an ion density that decreases with time and in a broad energy spectrum. Actually, not all the ions in the Tail remain at all times behind the Sail front, i.e. in the $x < X(t)$ region. This is related to maintaining a mechanical quasi-equilibrium for electrons during the acceleration. As the Sail is accelerated toward higher velocities, the radiation pressure decreases by the factor $(1 - \beta)/(1 + \beta)$. Thus, the field E_x must decrease by the same factor to keep the electrons in equilibrium. This is evident in figure 7, where we plot the peak field $E_m(t) = \max[E_x(x, t)] = E_x(x = X(t))$ and show that $E_m(t) \simeq E_m(0)(1 - \beta(t))/(1 + \beta(t))$, so that the pressure equilibrium is maintained. In 1D, the value of E_x at a point x' is proportional to the amount of charge contained in the $x < x'$ region; thus, there must be a positive current through the $x = X(t)$ surface during the acceleration stage. By computing the total number of ions in the $x > X(t)$ region, we find that there is a flow of ions in the forward direction at the

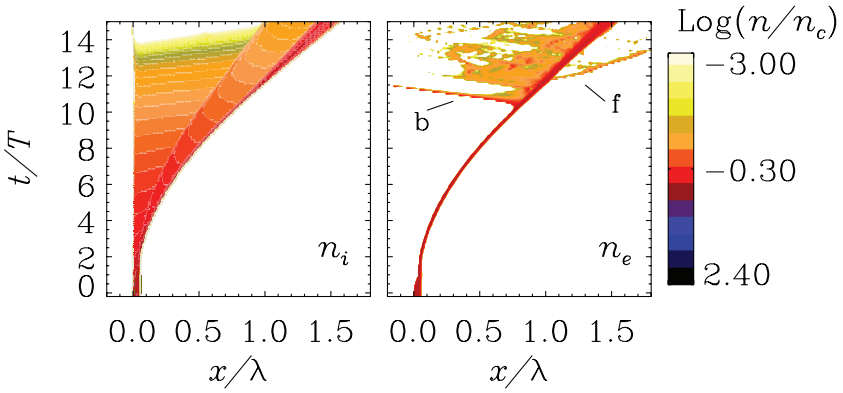

Figure 8. Space–time contours of $n_\mathrm{i} = n_\mathrm{i}(x,t)$ and $n_\mathrm{e} = n_\mathrm{e}(x,t)$ from the same simulation of figure 6, in logarithmic scale. Labels 'b' and 'f' indicate two electron bunches leaving the Sail in the backward and forward direction, respectively, at $t \simeq 11$.

$x = X(t)$ surface. These ions are accelerated by the space-charge field in the Tail region and overturn the position of the Sail front.

The number of electrons in the Sail remains constant up to near the end of the laser pulse, i.e. when the laser amplitude at the foil surface drops down. At a certain time, P_rad does not balance P_es anymore and thus electrons no longer remain in mechanical equilibrium. As a consequence, a bunch of electrons is accelerated *backward* by E_x, as shown in figure 6(b). Some other electrons leave the Sail at later times and also in the forward direction, acquiring a larger velocity than the Sail. This dynamics is best visualized by plotting the space–time contours of $n_\mathrm{i}(x,t)$ and $n_\mathrm{e}(x,t)$ in logarithmic scale, as in figure 8. The detachment of excess electrons eventually leaves the Sail neutral. At the same time, the loss of mechanical equilibrium causes heating of the electrons, driving in turn the expansion of the Sail (which can be noticed in figure 8) and the broadening of the ion spectrum.

Despite the formation of two ion populations, of which the 'monoenergetic' one may be less numerous, the fraction of laser pulse energy converted into kinetic energy of the ions is still in good agreement with the LS efficiency η given by equation (8), which in turn depends only on the Sail velocity. Since work has to be done by the laser pulse to push the negatively charged Sail against the electrostatic field E_x generated by the ions in the Tail, part of the energy is stored as electrostatic energy [28] and eventually converted into kinetic energy of ions in the Tail.

In a recent similar study, Eliasson *et al* [27] also noticed the formation of two ion populations. In their work, ions in the Sail are referred to as 'trapped' in an effective potential in the Sail frame. Using an argument of force balance (instead of pressure balance), they estimate the fraction of ions initially trapped as $F \simeq 1 - (a_0^2/\zeta^2)/2$.

4. 2D simulations

The analysis of the two preceding sections is based on a 1D approach, which may be accurate only under certain conditions, i.e. when the intensity distribution of the laser pulse in the focal plane is flat-top and the foil displacement is smaller than the focal spot radius. To check the predictions of the 1D model, we performed 2D simulations for laser and target parameters close

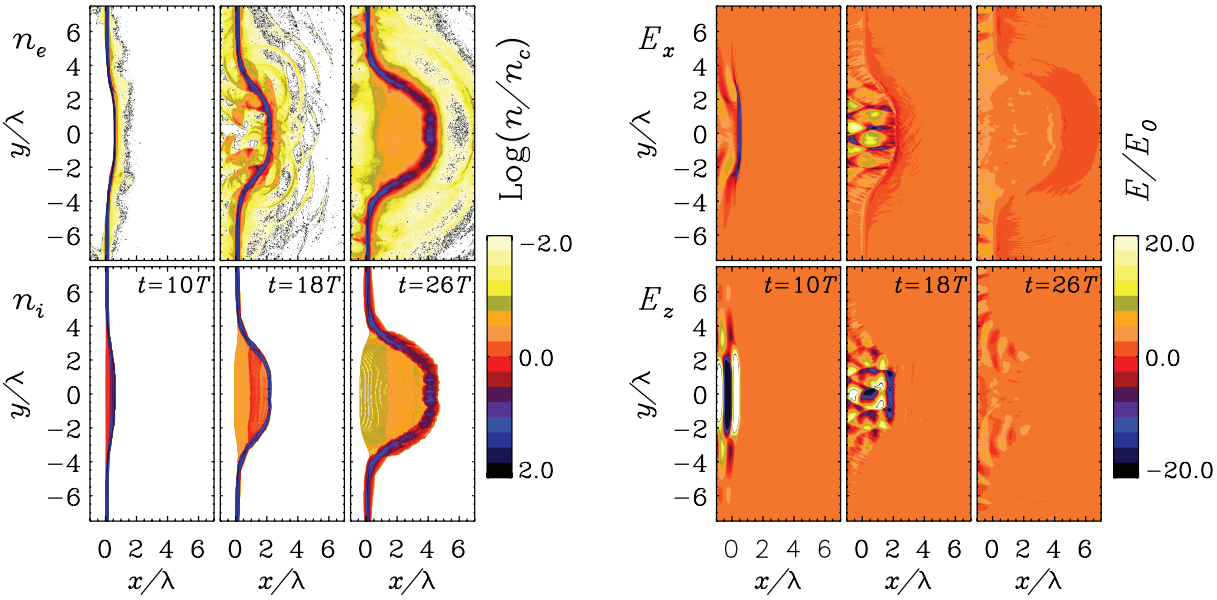

Figure 9. 2D simulation results. Snapshots of n_e, n_i and electric field components E_x and E_z are shown at three different times. The laser pulse has eight cycle duration and eight wavelength diameter (both FWHM) and peak amplitude $a_0 = 20$. The plasma foil has initial density $n_e = 50n_c$ and thickness $\ell = 0.2\lambda$. Normalizations are as in figure 6.

to the optimal thickness condition (24). In 2D geometry, several effects of possible relevance are taken into account, including e.g. laser intensity distribution, bending of the target, increased heating of electrons due to longitudinal components of the electric field out of the laser axis and onset of surface rippling instabilities. A few groups also reported 3D simulations of thin-foil RPA [4, 14, 24]. These simulations are generally very demanding numerically, also because, as shown by the 1D analysis, high values of the spatial resolution and of the number of particles per cell are needed to resolve the huge density variations in the plasma. With respect to the 2D case, in 3D geometry the additional physical constraint of the conservation of the angular momentum delivered by the circularly polarized laser pulse is taken into account. A theoretical analysis [24] shows that angular momentum absorption in the plasma may occur only via dissipative effects; thus, in general it does not provide the generation of an axial magnetic field, according to the mechanism hypothesized in [26].

Figure 9 shows snapshots of ion and electron densities and of E_x and E_z field components from 2D simulations. The laser pulse has a peak amplitude $a_0 = 20$ and a fourth-order supergaussian (i.e. an $\exp(-u^4)$ function) profile both in the longitudinal (x) and in the transverse (y) directions, with eight cycle duration and eight wavelength width (both FWHM). The foil target has initial electron density $n_e = 50n_c$ and thickness $\ell = 0.2\lambda$ so that $\zeta = 31.4$.

At the intermediate time $t = 18$, the formation of the low-density Tail of ions can be noticed in the contour plot of n_i. The electron density distribution is more complicated due to 2D effects. As the foil is accelerated by the laser pulse, owing to target deformation the laser pulse incidence is effectively oblique at the edges of the laser spot. Moreover, as soon as the foil displacement is a few times λ, the light reflected from one edge is incident back on the opposite

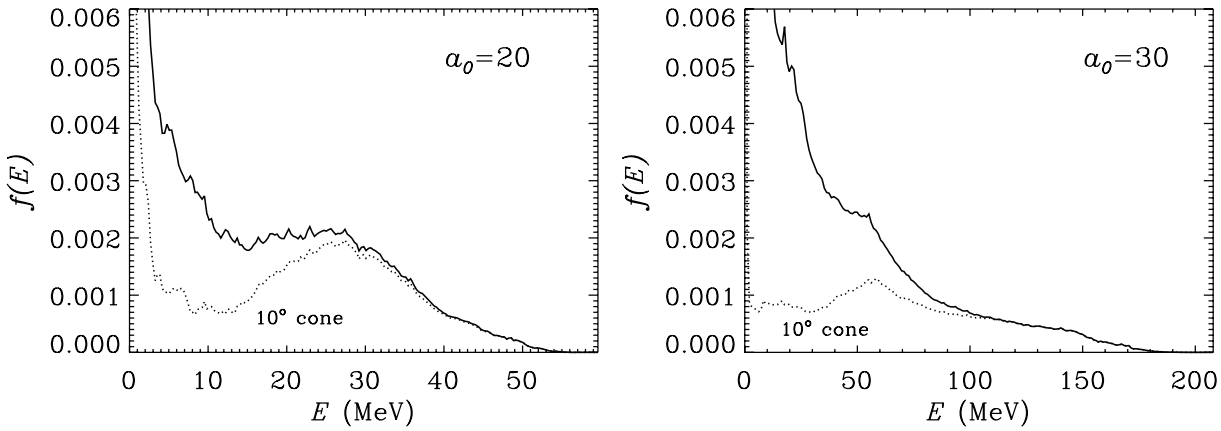

Figure 10. Ion spectra (in energy per nucleon) from the simulations of figure 9 ($a_0 = 20$) and figure 11 ($a_0 = 30$). The dotted line gives the spectrum where only ions inside a 10° cone around the axis are included. Both spectra correspond to the latest time in figures 9 and 11.

side, and a standing wave-like pattern is observed ($t = 18$ T). These effects enhance electron heating, driving the formation of a low-density electron cloud around the target and leading to broadening of the ion spectrum due to thermal expansion of the foil. In turn, absorption into electrons and oblique incidence reduce the radiation pressure at the edges of the focal spot, and may thus enhance the effect of the inhomogeneous distribution of the laser intensity. A similar dynamics is also noticed for even 'flatter' intensity profiles (e.g. eighth-order supergaussian).

As a likely consequence of stronger electron heating in 2D, the ion spectrum shown in figure 10 is quite broad, even when only ions moving into a 10° cone around the axis are considered. According to these results, to obtain a monoenergetic spectrum is a challenging issue. In two recent papers, Chen *et al* investigated strategies to improve monoenergeticity based on tailoring either the laser intensity distribution [12] or the thickness of the target [14].

It also appears that 2D effects make the optimal thickness condition (24) more stringent, so that a lower intensity is required. Figure 11 shows snapshots from simulations with the same parameters as in figure 9, but with the pulse amplitude $a_0 = 30$, close to the value of $\zeta = 31.4$. We observe a strong transmission of the laser pulse, causing a strong turbulence in the electron density. The strong transmission appears to be correlated with a strong rarefaction of the electron density out of the axis (around $y = \pm 2\lambda$ as in figure 11), leaving a denser bunch of ions along the axis. The corresponding spectrum shows that the RPA peak is barely distinguishable from the exponential-like background.

5. Conclusions

We reported an analytical and simulation study of RPA of ultrathin foils. The effects of the nonlinear SIT of the foil were addressed and incorporated into the 1D 'LS' model for foil acceleration. The model predictions for ion energy and conversion efficiency as a function of target thickness were in fairly good agreement with the result of 1D simulations. The latter were further analyzed to unfold the dynamics and self-organization of foil acceleration. 2D simulations for parameters close to the 'optimal' thickness value given by the 1D theory showed

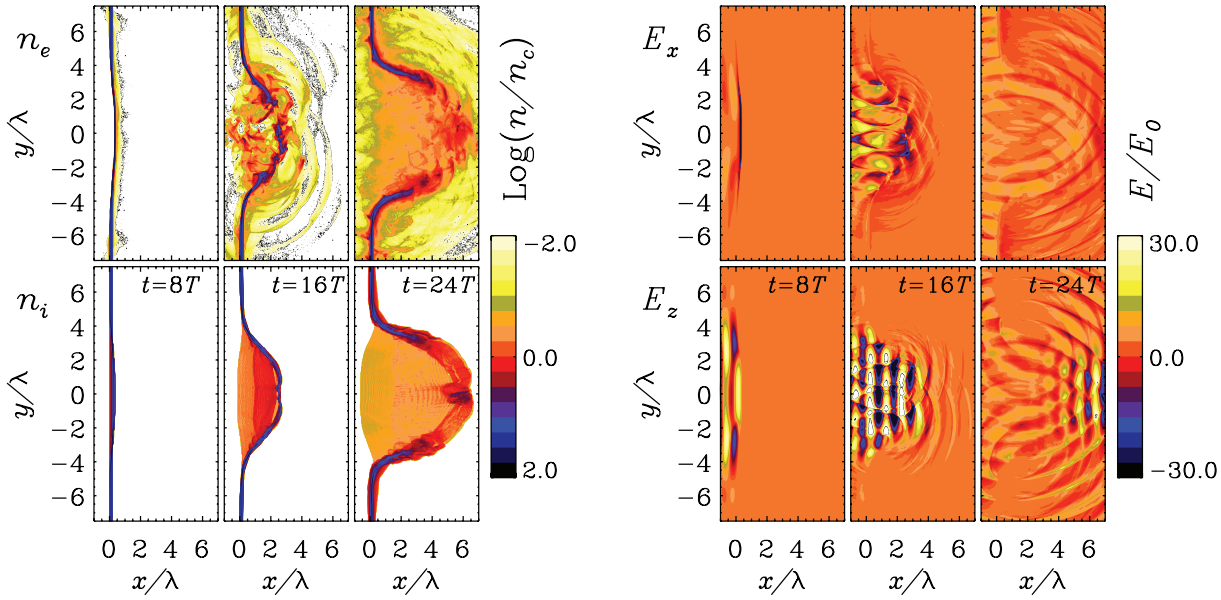

Figure 11. Same as figure 9, but for a pulse amplitude $a_0 = 30$.

that deformation of the target causes strong heating of electrons, leading to a broad ion spectrum and giving a lower threshold for the penetration of the laser pulse through the foil.

Acknowledgments

Support from CNR via an RSTL project and use of supercomputing facilities at CINECA (Bologna, Italy) sponsored by the CNR/INFM supercomputing initiative are acknowledged.

References

[1] Badziak J, Glowacz S, Jablonski S, Parys P, Wolowski J, Hora H, Krása J, Láska L and Rohlena K 2004 Production of ultrahigh ion current densities at skin-layer subrelativistic laser-plasma interaction *Plasma Phys. Control. Fusion* **46** B541–55

[2] Kar S *et al* 2008 Plasma jets driven by ultraintense-laser interaction with thin foils *Phys. Rev. Lett.* **100** 225004

[3] Akli K U *et al* 2008 Laser heating of solid matter by light-pressure-driven shocks at ultrarelativistic intensities *Phys. Rev. Lett.* **100** 165002

[4] Esirkepov T, Borghesi M, Bulanov S V, Mourou G and Tajima T 2004 Highly efficient relativistic-ion generation in the laser-piston regime *Phys. Rev. Lett.* **92** 175003

[5] Esirkepov T, Yamagiwa M and Tajima T 2006 Laser ion-acceleration scaling laws seen in multiparametric particle-in-cell simulations *Phys. Rev. Lett.* **96** 105001

[6] Pegoraro F and Bulanov S V 2007 Photon bubbles and ion acceleration in a plasma dominated by the radiation pressure of an electromagnetic pulse *Phys. Rev. Lett.* **99** 065002

[7] Borghesi M, Fuchs J, Bulanov S V, MacKinnon A J, Patel P K and Roth M 2006 Fast ion generation by high-intensity laser irradiation of solid targets and applications *Fus. Sci. Technol.* **49** 412

[8] Macchi A, Cattani F, Liseykina T V and Cornolti F 2005 Laser acceleration of ion bunches at the front surface of overdense plasmas *Phys. Rev. Lett.* **94** 165003

[9] Liseikina T V and Macchi A 2007 Features of ion acceleration by circularly polarized laser pulses *Appl. Phys. Lett.* **91** 171502
[10] Robinson A P L, Gibbon P, Zepf M, Kar S, Evans R G and Bellei C 2009 Relativistically correct hole-boring and ion acceleration by circularly polarized laser pulses *Plasma Phys. Control. Fusion* **51** 024004
[11] Naumova N, Schlegel T, Tikhonchuk V T, Labaune C, Sokolov I V and Mourou G 2009 Hole boring in a DT pellet and fast-ion ignition with ultraintense laser pulses *Phys. Rev. Lett.* **102** 025002
[12] Chen M, Pukhov A, Sheng Z M and Yan X Q 2008 Laser mode effects on the ion acceleration during circularly polarized laser pulse interaction with foil targets *Phys. Plasmas* **15** 113103
[13] Yin Y, Yu W, Yu M Y, Lei A, Yang X, Xu H and Senecha V K 2008 Influence of target thickness on the generation of high-density ion bunches by ultrashort circularly polarized laser pulses *Phys. Plasmas* **15** 093106
[14] Chen M, Pukhov A, Yu T P and Sheng Z M 2009 Enhanced collimated GeV monoenergetic ion acceleration from a shaped foil target irradiated by a circularly polarized laser pulse *Phys. Rev. Lett.* **103** 024801
[15] Zhang X, Shen B, Ji L, Wang F, Jin Z, Li X, Wen M and Cary J R 2009 Ion acceleration with mixed solid targets interacting with circularly polarized lasers *Phys. Rev. Sel. Top. Accel. Beams* **12** 021301
[16] Robinson A P L, Kwon D-H and Lancaster K 2009 Hole-boring radiation pressure acceleration with two ion species *Plasma Phys. Control. Fusion* **51** 095006
[17] Gonoskov A A, Korzhimanov A V, Eremin V I, Kim A V and Sergeev A M 2009 Multicascade proton acceleration by a superintense laser pulse in the regime of relativistically induced slab transparency *Phys. Rev. Lett.* **102** 184801
[18] Grech M, Skupin S, Nuter R, Gremillet L and Lefebvre E 2009 High-quality ion beams by irradiating a nano-structured target with a petawatt laser pulse *New J. Phys.* **11** 093035
[19] Zhang X, Shen B, Li X, Jin Z and Wang F 2007 Multistaged acceleration of ions by circularly polarized laser pulse: monoenergetic ion beam generation *Phys. Plasmas* **14** 073101
[20] Zhang X, Shen B, Li X, Jin Z, Wang F and Wen M 2007 Efficient GeV ion generation by ultraintense circularly polarized laser pulse *Phys. Plasmas* **14** 123108
[21] Robinson A P L, Zepf M, Kar S, Evans R G and Bellei C 2008 Radiation pressure acceleration of thin foils with circularly polarized laser pulses *New J. Phys.* **10** 013021
[22] Klimo O, Psikal J, Limpouch J and Tikhonchuk V T 2008 Monoenergetic ion beams from ultrathin foils irradiated by ultrahigh-contrast circularly polarized laser pulses *Phys. Rev. Sel. Top. Accel. Beams* **11** 031301
[23] Yan X Q *et al* 2008 Generating high-current monoenergetic proton beams by a circularly polarized laser pulse in the phase-stable acceleration regime *Phys. Rev. Lett.* **100** 135003
[24] Liseykina T V, Borghesi M, Macchi A and Tuveri S 2008 Radiation pressure acceleration by ultraintense laser pulses *Plasma Phys. Control. Fusion* **50** 124033
[25] Qiao B, Zepf M, Borghesi M and Geissler M 2009 Stable GeV ion-beam acceleration from thin foils by circularly polarized laser pulses *Phys. Rev. Lett.* **102** 145002
[26] Tripathi V K, Liu C S, Shao X, Eliasson B and Sagdeev R Z 2009 Laser acceleration of monoenergetic protons in a self-organized double layer from thin foil *Plasma Phys. Control. Fusion* **51** 024014
[27] Eliasson B, Liu C S, Shao X, Sagdeev R Z and Shukla P K 2009 Laser acceleration of monoenergetic protons via a double layer emerging from an ultra-thin foil *New J. Phys.* **11** 073006
[28] Macchi A, Veghini S and Pegoraro F 2009 'Light Sail' acceleration reexamined *Phys. Rev. Lett.* **103** 085003
[29] Yan X Q, Wu H C, Sheng Z M, Chen J E and Meyer–ter–Vehn J 2009 Self-organizing GeV, nanocoulomb, collimated proton beam from laser foil interaction at 7×10^{21} W cm^{-2} *Phys. Rev. Lett.* **103** 135001
[30] Rykovanov S G, Schreiber J, Meyer–ter–Vehn J, Bellei C, Henig A, Wu H C and Geissler M 2008 Ion acceleration with ultra-thin foils using elliptically polarized laser pulses *New J. Phys.* **10** 113005
[31] Macchi A, Liseikina T V, Tuveri S and Veghini S 2009 Theory and simulation of ion acceleration with circularly polarized laser pulses *C. R. Phys.* **10** 207–15
[32] Borghesi M 2009 Talk at the *Coulomb09 Workshop Ion Acceleration with High Power Lasers: Physics and Applications (Senigallia, Italy, June 15–18, 2009)*

[33] Yan X 2009 Talk at the *Coulomb09 Workshop Ion Acceleration with High Power Lasers: Physics and Applications (Senigallia, Italy, June 15–18, 2009)*
[34] Henig A *et al* 2009 Radiation-pressure acceleration of ion beams driven by circularly polarized laser pulses *Phys. Rev. Lett.* **103** 245003
[35] Thaury C *et al* 2007 Plasma mirrors for ultrahigh-intensity optics *Nat. Phys.* **3** 424–9
[36] Marx G 1966 Interstellar vehicle propelled by terrestrial laser beam *Nature* **211** 22–3
[37] Simmons J F L and McInnes C R 1993 Was Marx right? or How efficient are laser driven interstellar spacecraft? *Am. J. Phys.* **61** 205–7
[38] Vshivkov V A, Naumova N M, Pegoraro F and Bulanov S V 1998 Nonlinear electrodynamics of the interaction of ultra-intense laser pulses with a thin foil *Phys. Plasmas* **5** 2727–41
[39] Veghini S 2009 A model for thin foil acceleration by laser pulses *Master's Thesis* University of Pisa 2009 [In Italian]
[40] Landau L and Lifshitz E M 1962 *The Classical Theory of Fields* 2nd edn (Oxford: Pergamon Press) chapter 78 p 250
[41] Ji L, Shen B, Zhang X, Wang F, Jin Z, Wen M, Wang W and Xu J 2009 Comment on Generating high-current monoenergetic proton beams by a circularly polarized laser pulse in the phase-stable acceleration regime *Phys. Rev. Lett.* **102** 239501
[42] Yan X Q, Lin C, Sheng Z M, Guo Z Y, Liu B C, Lu Y R, Fang J X and Chen J E 2009 Comment on Generating high-current monoenergetic proton beams by a circularly polarized laser pulse in the phase-stable acceleration regime *Phys. Rev. Lett.* **102** 239502